Compact micro-optic based components for hollow core fibers

YONGMIN JUNG,[1,*] HYUNTAI KIM,[1,2,**] YONG CHEN,[1] THOMAS D. BRADLEY,[1] IAN A. DAVIDSON,[1] JOHN R. HAYES,[1] GREGORY JASION,[1] HESHAM SAKR,[1] SHUICHIRO RIKIMI,[1] FRANCESCO POLETTI,[1] AND DAVID J. RICHARDSON[1]

[1]*Optoelectronics Research Centre, University of Southampton, Southampton, SO17 1BJ, UK*
[2] *Current address: Electrical and Electronic Convergence Department, Hongik University, Sejong, 30016, Republic of Korea.*
**ymj@orc.soton.ac.uk and **hyuntai@hongik.ac.kr*

Abstract: Using micro-optic collimator technology, we present compact, low-loss optical interconnection devices for hollow core fibers (HCFs). This approach is one of the key manufacturing platforms for commercially available fiber optic components and most forms of HCFs can readily be incorporated into this platform without the need for any substantial or complicated adaptation or physical deformation of the fiber structure. Furthermore, this technique can provide for very low Fresnel reflection interconnection between solid-core fiber and HCF and in addition provides a hermetic seal for HCFs, which can be a critical issue for many HCF applications. In this paper, several exemplar HCF components are fabricated with low insertion loss (0.5-2 dB), low Fresnel reflection (-45 dB) and high modal purity (>20 dB) using various state-of-the-art HCFs.

1. Introduction

Hollow core fibers (HCFs), which guide light in air or a vacuum within a hollow core, have attracted great interest as a promising means to overcome various limitations associated with conventional solid core fibers in which the light propagates within glass [1-3]. Several different types of HCF (e.g. photonic bandgap fibers and anti-resonant fibers such as Tubular and Kagome fibers) have been proposed to exploit the fascinating features of guidance in an air core (e.g. low nonlinearity, low Rayleigh scattering, low latency, good thermal stability, high damage threshold and high radiation hardness) and such fibers have shown excellent performance in applications such as optical communications, high power laser beam delivery, gyroscopes, sensors and Raman spectroscopy [4-10]. However, whilst such fibers have been available for several years, there is still a lack of reliable interconnection techniques for HCF technology and an associated lack of integrated HCF components. Fusion splicing is the most widely used approach to interconnect a HCF to a conventional single mode fiber (SMF) but unless other steps are taken this results in a strong Fresnel reflection (typically ~4%) at the SMF-HCF air-glass interface which can be problematic for many applications. Angle-cleaved fiber splicing (i.e. incorporating angle cleaving for both the HCF and solid core fiber) has been proposed to suppress such back reflection [11] however the output beam direction from the angle-cleaved solid fiber is deflected from the fiber axis in the process, resulting in increased splice loss and the excitation of higher-order HCF modes which can be problematic in many instances. In addition, the mode field diameters (MFDs) of the HCFs are larger than those of typical SMFs and appropriate mode field adaptation techniques are often required to minimize loss and to ensure high purity excitation of the fundamental mode [12, 13]. Up to now, only a few HCF components have become commercially available and the majority of these are for fiber termination or connectorization only. Due to this, the use of solid-core fiber optic components (e.g. couplers, isolators, polarizers etc.) is the only available solution for many HCF applications, requiring solid-core fiber to HCF splicing which generally degrades

performance (e.g. through increased losses, due to splicing, and/or back reflections, due to the 4% Fresnel reflection from flat air/glass interfaces). Moreover, this often necessitates the use of very short pigtail lengths to minimize the impact of the solid-core fiber properties themselves.

In this paper, we propose and experimentally demonstrate a number of compact air gap devices using micro-optic collimator technology for SMF-HCF and HCF-HCF interconnection. Such a platform has been widely used previously for the development of various solid core fiber coupled components [14] and we further investigate the use of micro-optic collimator technology with HCFs. After introducing the basic structure of the micro-collimator device, we construct various 2-port HCF components (e.g. isolators and band-pass filters) and describe the detailed fabrication procedure and optical characterization. Finally, we further extend our work to multiport HCF devices and demonstrate several exemplar in-line 3-port HCF components which exhibit low insertion loss, good modal quality and low Fresnel reflections.

2. 2-port HCF components

2.1 SMF-HCF device

Figure 1(a) shows a schematic of the proposed 2-port HCF interconnection device– in particular between a solid core fiber (SCF) and a hollow core fiber (HCF) [15]. Using a commercially available compact micro-collimator platform (i.e. low loss, low cost with highly reliable fabrication tools and parts available to make a wide range of fiber optic components such as optical isolators, circulators, beam splitters and switches), light emerging from the input SCF was collimated in free space and then efficiently coupled into the output HCF with a low insertion loss. Importantly, these micro-lenses (typically C-lens or GRIN lens) are available with an 8º facet angle and hence a very low Fresnel reflection between SCF and HCF can be achieved by incorporating an angle-cleaved SCF at the input end. In order to explore the benefits of this micro-optic collimator platform, an in-house made 19-cell hollow-core photonic bandgap fiber (PBGF) [16] was used as an exemplary HCF in our first experiment. Figure 1(b) shows a cross section of the fiber used. The fiber has a core diameter of 30 µm, a micro-structured cladding diameter of 84 µm and a cladding diameter of 230 µm. The fiber attenuation is ~3.9 dB/km at 1550 nm. Note that this particular fiber is inherently few-moded (i.e. it supports several higher-order guided modes (from the LP_{11} up to LP_{02} mode groups) over a few hundred meters of fiber) and special attention was paid to the lateral positioning of the two fibers so to excite predominantly the fundamental mode in this fiber. As an input fiber, a solid-core large mode area (LMA) fiber having a similar MFD to our HCF (~21 µm) was used and a mode field adaptor (MFA) [12, 13] was incorporated to reduce the splice loss between a length of conventional single mode fiber (e.g. SMF-28) (the input pigtail fiber) and the LMA fiber. Ceramic fiber ferrules with a slightly bigger hole (diameter=250 µm) were used to accommodate our HCF and a pair of C-lenses (diameter=1.8 mm, focal length=2.98 mm) was employed for efficient fiber-to-fiber coupling. Precise lateral alignment was provided by a pair of five-axis precision micro-stage and active optical alignment using a time-of-flight measurement (i.e. impulse response measurement) [17] was used to minimize unwanted higher-order mode (HOM) excitation and to achieve maximum coupling efficiency to the fundamental mode. Once the collimator alignment was optimized the collimators were glued into place using a suitable UV curable epoxy within a protective glass tube and this was then protected itself through further packaging steps. Figure 1(c) shows a photograph of a fully-assembled 2-port HCF prototype device. The two fiber collimators are hermetically-sealed inside a protective glass tube and a further metal housing is added for increased mechanical protection. The total device length is ~7 cm.

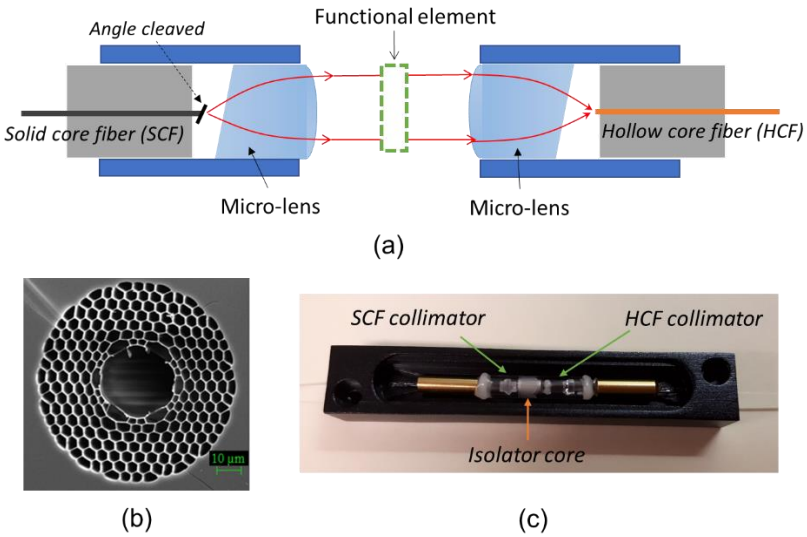

Fig. 1. (a) A schematic of 2-port hollow-core fiber components based on micro-optic collimator assembly, (b) a cross-section scanning electron microscope (SEM) image of a 19-cell hollow-core photonic bandgap fiber and (c) photograph of the packaged HCF device.

The insertion loss of the device was measured first with a C-band amplified spontaneous emission (ASE) light source and power meter. The total interconnection loss from the SMF input to HCF output was measured to be 0.53 dB – where the loss contribution from the SMF-LMA fiber connection with an MFA was 0.28 dB and the loss from the LMA fiber-HCF micro-collimator device itself was 0.25 dB. We then measured the back reflection of the fabricated device and confirmed that it is very low (-49.8 dB) since there is no flat glass/air interface within the entire optical path. This ensures that such HCF devices are compatible with many high sensitivity sensor, spectroscopy and gyroscope applications. We also tested the modal quality after the device using a time-of-flight measurement and less than -20 dB of higher-order mode content was observed compared to the fundamental mode (-21.2 dB for LP_{11} and -22.1 dB for LP_{02}). Note that this value is much better than for a SMF-HCF butt coupled joint (typically around -13 dB for LP_{02}) due to the better match between the MFDs. Importantly, the current mode quality could be further improved by placing another such micro-optic collimator assembly at the output end of the HCF (i.e. an identical device but for the interconnection from HCF to SMF).

In order to realize a practical HCF components, a functional element (e.g. isolator, filter, polarizer, etc.) can be placed in the air-gap between the two micro-optic collimators. Here, we have implemented an optical isolator inside the device. The total device loss was 1.5 dB and the back reflection was -47 dB. As shown in Fig. 2(a), the average optical isolation was more than 30 dB over the full C-band and the maximum peak optical isolation was >40 dB at 1552 nm. Note that the value of optical isolation is, to a large extent, determined by the isolator core material itself (more precisely, the thickness accuracy of the Faraday rotator used) [18-19]. The detailed characteristics of the basic SMF-HCF air-gap device are summarized in Fig. 2(b), where the properties of the interconnection device are shown above the solid line and the properties of the SMF-HCF isolator are shown below. It is also worth noting that we have tested the long-term stability of the device for 4 months and no performance degradation was observed due to the near hermetic seal obtained from the glass mounting tubes and the UV curable epoxies used in packaging the device.

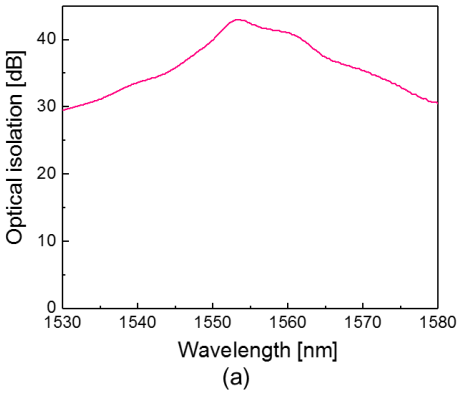

Parameter	Value
Fiber type	SMF/PBGF
Operation wavelength	C-band
Insertion loss	0.53 dB
HOM intensity	<-20 dB
Back reflection	-49.8 dB
Insertion loss (Isolator)	1.5 dB
Isolation @C-band	>30 dB

(b)

Fig. 2. (a) Optical isolation spectrum of SMF-HCF isolator and (b) summary specification of SMF-HCF device.

2.2 HCF-HCF device

As another example of 2-port HCF devices, an in-line fiber optic band-pass filter (BPF) was fabricated between two HCFs. In general, HCF to HCF interconnection is less problematic compared to SCF-HCF interconnection, because it represents a simple interconnection between two identical fibers and the Fresnel back reflections are negligible as there are no glass/air interfaces (except for the anti-reflection coated micro-lenses). The schematic of the HCF-HCF device is almost the same as for the previous SMF-HCF interconnection device except that two identical HCFs (i.e. the same 19-cell PBGF in Fig. 1b) are used as input/output fibers. The HCF-HCF interconnection loss was measured to be ~1.28 dB and good modal purity (>20 dB) was observed. Note that all our device performance are measured/defined after the final packaging (not after the optical alignment process) and the insertion loss varies from device to device but we can readily fabricate micro-optic HCF devices with typical insertion loss of 1 dB to 1.5 dB. To provide an exemplar functional device a band-pass filter chip (having a 3 dB bandwidth of ~7 nm and a center wavelength of 1548 nm) was inserted within the air gap of the HCF-HCF interconnection assembly. The total device loss was slightly increased to 1.85 dB, including the insertion loss of the BPF chip itself. The measured optical spectra before and after the BPF are shown in Fig. 3(a). A HCF coupled flat-top single-band BPF was obtained with a minimum passband-to-rejection band ratio of 60 dB. The specification of the HCF-HCF interconnection device is summarized in Fig. 3(b) (the properties above the solid line are for the interconnection device and under the solid lines are for the HCF-HCF BPF).

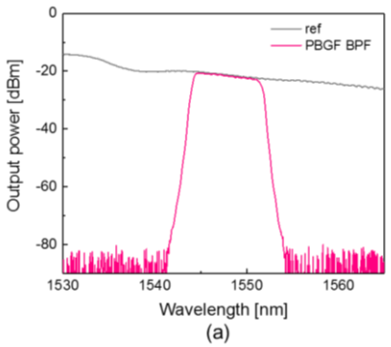

Parameter	Value
Fiber type	PBGF
Operation wavelength	C-band
Insertion loss	1.28 dB
HOM intensity	<-20 dB
Insertion loss (BPF)	1.85 dB
Center wavelength	1548 dB
3dB bandwidth	7 nm

(b)

Fig. 3. (a) Measured optical spectra before and after the band-pass filter and (b) summary specification of the HCF-HCF device.

3. 3-port HCF components

Figure 4(a) shows a schematic of a 3-port HCF device based on our micro-optic collimator assembly [20], which comprised a dual fiber collimator (left), a single fiber collimator (right) with a functional element in the middle. To prove the concept, we used a 50/50 dielectric beam splitter chip (dimension=1.4 mm × 1.4 mm) to make a 3 dB beam splitter, and a dichroic mirror to make a wavelength division multiplexing (WDM) coupler. In order to make these 3-port HCF devices, we first fabricated a dual fiber collimator using HCFs (left assembly in Fig. 4a). Two flat cleaved HCFs were inserted into a 500 µm-hole ceramic fiber ferrule and placed at the focal point of a short graded-index (GRIN) lens (pitch length=0.25, effective focal length=1.99 mm) to create collimated beams. Next, a 50/50 beam splitter chip was placed on a high precision flexure stage and actively aligned to a high degree of accuracy by monitoring the reflected power (Port1 →Port2). We used a GRIN lens with a flat surface in the dual fiber collimator to allow ready placement and final attachment of the mirror. In a second step, we assembled a single HCF collimator (right assembly in Fig. 4a), to produce a well collimated beam, this time using a C-lens (focal length=2.98 mm). Finally, these two collimator assemblies were combined together to realize our 3-port HCF device. Again precise active alignment was used to guarantee low loss interconnection from port1 to port3. In this work, we have used another state-of-the-art exemplar HCF, a nested anti-resonant nodeless fiber (NANF). A cross-sectional microscope image of the fiber is shown in Fig. 4(b). Six double nested capillaries form an anti-resonant cladding to provide efficient, low loss light guidance in the second anti-resonance window. The fiber [21] has a core diameter of 34 µm, a micro-structured cladding diameter of 90.6 µm and an outer diameter of 238 µm. The fiber loss was ~ 2.8 dB/km at 1550 nm and the fiber has a >300 nm transmission bandwidth. Note that this particular fiber supports effective single mode guidance, however if higher-order modes are excited at the input (particularly the LP_{11} mode) they can survive to a detectable level over short fiber lengths (e.g. a few meters to a few tens of meters) despite the relatively high differential modal loss associated with these fibers. We have examined the modal properties of this fiber in some detail, as will be discussed later when describing the performance of the fabricated HCF devices.

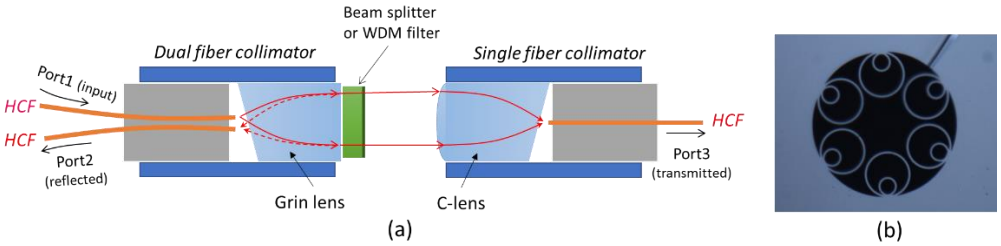

Fig. 4. (a) A schematic of 3-port HCF components based on micro-optic collimator assembly and (b) cross-sectional image of a nested anti-resonant nodeless fiber (NANF).

Figure 5(a) shows the reflection and transmission spectra of the fabricated (1×2) HCF-integrated beam splitter, which we measured using a super-luminescent diode and an optical spectrum analyzer. The power splitting ratio is relatively equal from 1500 nm to 1620 nm and the excess loss was measured to be ~2 dB including the insertion loss of the splitter chip (~0.5 dB). Here, the particular split-ratio is defined by the beam splitter chip used in our experiment and any desired split-ratio could be readily achieved through a different choice of dielectric beam splitter. For the reflection port (Port 2), a slight oscillatory spectral response is observed. We attribute this to intermodal interference resulting from the excitation of a small higher order mode (HOM) component at the reflection port originating from imperfect fiber collimator alignment coupled with the use of a short (few meter) HCF pigtail which was insufficient to suppress all HOM content. We note that these HOMs can be eliminated either through the use

of a longer fiber length (benefiting from the substantially higher loss of HOMs versus the fundamental), or if the short tails are tightly looped or bent (exploiting the increased bend loss sensitivity of HOMs).

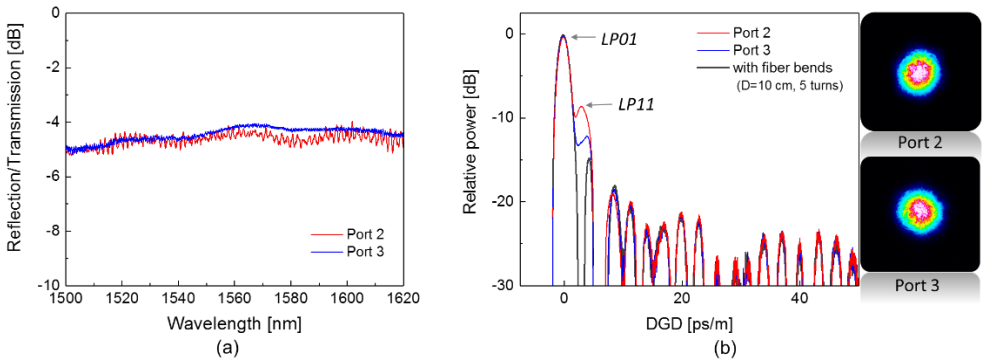

Fig. 5. (a) Reflection and transmission spectra of the fabricated HCF (1×2) beam splitter and the impulse response after propagating a 30 m of HCF with beam profiles from two output ports.

In order to visually assess the beam quality of the fabricated HCF (1×2) beam splitter, both output ports were first examined using a charge-coupled device (CCD). As shown in Fig. 5(b), quite clean fundamental mode profiles were observed at both fiber ports. However, note that such CCD beam profiling can only really be used only for quick identification of the dominant spatial modes, not quantitative modal analysis. Therefore, we further analyzed the modal quality of the device through a time-of-flight measurement by splicing an additional 30 m of HCF to the output, which enables enough intermodal delay to be discernible in the time domain. As shown in Fig. 5(b), a small LP_{11} peak can be identified at a differential group delay (DGD) of 2.6 ps/m and modal purity of the outputs was estimated to be ~8.4 dB for port 2 and ~12 dB for port 3, respectively. Note that the modal purity of the device depends crucially on the fiber alignment during the assembly and the center-to-center fiber alignment is critical to minimize this inter-modal crosstalk. However, as mentioned before, these HOMs can be effectively suppressed by bending the fiber without significantly affecting the LP_{01} mode loss and a high purity LP_{01} mode (>20 dB extinction ratio) is readily achieved with optimum fiber bending (e.g. bend diameter=10 cm, 5 turns) as shown in the gray colored trace in Fig. 5(b). Here, the LP_{11} modal peak at DGD=2.6 ps/m is seen to be completely eliminated and only detector ringing artifacts associated with the impulse response of the detector can be observed. Moreover, this HOM suppression can also be realized by employing a longer length of fiber and we have confirmed this by splicing an extra 160 m length of HCF on a fiber bobbin (diameter=30 cm) to output port 2 and observing that >20 dB modal purity can be readily achieved. We also measured the back reflection of the fabricated device and confirmed that it remains very low (<-45 dB).

As another example of a 3-port HCF device, we have fabricated a WDM coupler using a dichroic mirror chip (e.g. a C/L-band splitter in our demonstration) placed between two HCF collimators. This chip is commercially designed to be used for the splitting of telecom C-band (reflection from 1500 to 1564 nm) and L-band (transmission from 1570 to 1620 nm) channels. This WDM functionality is readily integrated into HCF devices as shown in Fig. 6. The excess loss of the HCF-WDM coupler was ~2 dB at both C- and L-bands (including the insertion loss of the dichroic mirror (~0.6 dB)). We can see a small signature of sinusoidal spectral fluctuation in the L-band, which is mainly due to thin-film interference effects associated with the dichroic mirror used. Note that such HCF-WDM couplers should prove very useful in many laser and amplifier configurations (especially, gas or dye lasers in HCF), Raman spectroscopy and pump-probe applications using HCFs [22, 23].

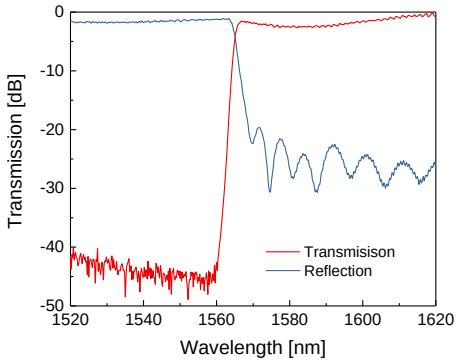

Fig. 6. Reflection and transmission spectra of WDM coupler for HCFs.

4. Conclusion

We have incorporated hollow-core fibers (HCFs) in a compact micro-optic collimator assembly (having a micro-lens diameter of 1.8 mm) and successfully developed various practical HCF components (e.g. optical isolator, band-pass filter, 1×2 beam splitter and WDM coupler), which provides a robust, diverse and enabling platform to incorporate various optical functionalities into HCF systems. Importantly, this approach not only provides for very low Fresnel reflections from the interconnection between solid core fiber and HCF, but can also offer an effective hermetic seal for HCFs as needed to protect from unwanted ingression of gases and particles. All fabricated devices show very good optical performance with a low insertion loss (0.5-2 dB), low back reflection (<-45 dB) and a high modal purity (>20 dB). These compact, reliable and low-loss interconnection platforms for HCFs can be further optimized and integrated within more complex devices/systems and promise to provide valuable technology in support of various aspects of HCF related research.

Acknowledgments

This work was supported in part by the EPSRC funded "Airguide Photonics" Programme Grant (EP/P030181/1), the EPSRC National Hub in High Value Photonic Manufacturing (EP/N00762X/1), the EPSRC Impact Acceleration Account Award (EP/R511766/1) and ERC Lightpipe project (682724). Data published in this paper are available from the University of Southampton repository at http://doi.org/10.5258/SOTON/D1143.

Disclosures

The authors declare no conflicts of interest.

References

1. R. Cregan, B. Mangan, J. Knight, T. Birks, P. S. J. Russell, P. Roberts, and D. Allan, "Single-mode photonic band gap guidance of light in air," Science **285**, 1537-1539 (1999).
2. P. Russell, "Photonic crystal fibers," Science **299**, 358-362 (2003).
3. F. Poletti, N. Wheeler, M. Petrovich, N. Baddela, E. N. Fokoua, J. Hayes, D. Gray, Z. Li, R. Slavík, and D. Richardson, "Towards high-capacity fibre-optic communications at the speed of light in vacuum," Nat. Photonics **7**, 279 (2013).
4. F. Poletti, M. N. Petrovich, and D. J. Richardson, "Hollow-core photonic bandgap fibers: technology and applications," Nanophotonics **2**, 315-340 (2013).
5. M. Michieletto, J. K. Lyngsø, C. Jakobsen, J. Lægsgaard, O. Bang, and T. T. Alkeskjold, "Hollow-core fibers for high power pulse delivery," Opt. Express **24**, 7103-7119 (2016).

6. F. Benabid, J. C. Knight, G. Antonopoulos, P. St. J. Russel, “Stimulated Raman scattering in hydrogen-filled hollow-core photonic crystal fiber,” Science **298**, 399-402 (2002).
7. P. St. J. Russel, P. Holzer, W. Chang, A. Abdolvand and J. C. Travers, “Hollow-core photonic crystal fibres for gas-based nonlinear optics,” Nat. Photonics **8**, 278-286 (2014).
8. S. Blin, H. K. Kim, M. J. Digonnet, and G. S. Kino, “Reduced thermal sensitivity of a fiber-optic gyroscope using an air-core photonic-bandgap fiber,” J. Lightwave Technol. **25**, 861-865 (2007).
9. Y. Wang, X. Peng, M. Alharbi, C. F. Dutin, T. Bradley, F. Gérôme, M. Mielke, T. Booth, and F. Benabid, “Design and fabrication of hollow-core photonic crystal fibers for high-power ultrashort pulse transportation and pulse compression,” Opt. Lett. **37**, 3111-3113 (2012).
10. J. R. Hayes, S. R. Sandoghchi, T. D. Bradley, Z. Liu, R. Slavík, M. A. Gouveia, N. V. Wheeler, G. Jasion, Y. Chen, E. N. Fokoua *et al.*, “Antiresonant hollow core fiber with an octave spanning bandwidth for short haul data communications,” J. Lightwave Technol. **35**, 437-442 (2017).
11. F. Couny, F. Benabid, and P. Light, “Reduction of fresnel back-reflection at splice interface between hollow core PCF and single-mode fiber,” IEEE Photonics Technol. Lett. **19**, 1020-1022 (2007).
12. P. Hofmann, A. Mafi, C. Jollivet, T. Tiess, N. Peyghambarian and A. Schülzgen, “Detailed investigation of mode-field adapters utilizing multimode-interference in graded index fibers”, J. Lightwave Technol. **30**, 2289-2298 (2012).
13. Y. Jung, J. Hayes, Y. Sasaki, K. Aikawa, S. U. Alam, and D. J. Richardson, “All-fiber optical interconnection for dissimilar multicore fibers with low insertion loss,” in Proc. of OFC 2017, paper W3H.2.
14. Y. Jung, A. Wood, S. Jain, Y. Sasaki, S.-U. Alam, and D. J. Richardson, “Fully integrated optical isolators for space division multiplexed (SDM) transmission,” APL Photonics **4**, 022801 (2019).
15. H. Kim, Y. Jung, Y. Chen, S. Rikimi, F. Poletti, and D. J. Richardson, "Free Space based Hollow Core Fiber Interconnection and Associated In-Line Components," in Proc. of OFC 2019, paper Th3E.3.
16. Y. Chen, Z. Liu, S. R. Sandoghchi, G. T. Jasion, T. D. Bradley, E. N. Fokoua, J. R. Hayes, N. V. Wheeler, D. R. Gray, B. J. Mangan, R. Slavík, F. Poletti, M. N. Petrovich, and D. J. Richardson, “Multi-kilometer Long, Longitudinally Uniform Hollow Core Photonic Bandgap Fibers for Broadband Low Latency Data Transmission,” J. Lightwave Technol. **34**, 104-113 (2016).
17. V. A. J. M. Sleiffer et al., “High Capacity Mode-Division Multiplexed Optical Transmission in a Novel 37-cell Hollow-Core Photonic Bandgap Fiber,” J. Lightwave Technol. **32**, 854-863 (2014).
18. H. Iwamura, S. Hayashi, H. Iwasaki, “A compact optical isolator using a Y3Fe5O12 crystal for near infra-red radiation,” Opt. Quantum Electron. **10**, 393-398 (1978).
19. D. L. Wood and J. P. Remeika, “Effect of impurities on the optical properties of Yttrium Iron Garmet,” J. Appl. Phys. **38**, 1038 (1967).
20. Y. Jung, T. D. Bradley, J. R. Hayes, G. Jasion, I. A. Davidson, H. Sakr, Y. Chen, F. Poletti, D. J. Richardson, “Multiport micro-optic devices for hollow core fibre applications,” in Proc. of ECOC 2019, paper Tu.2.E.4.
21. T. D. Bradley, J. R. Hayes, Y. Chen, G. T. Jasion, S. R. Sandoghchi, R. Slavik, E. N. Fokoua, S. Bawn, H. Sakr, I. A. Davidson, A. Taranta, J. P. Thomas, M. N. Petrovich, D. J. Richardson and F. Poletti, “Record low-loss 1.3 dB/km data transmitting antiresonant hollow core fiber,” in Proc. of ECOC 2018, Paper Th3F.2.
22. F. Couny, F. Benabid and P. S. Light, “Subwatt threshold cw Raman fiber-gas laser based on H2-filled hollow-core photonic crystal fiber,” Phy. Rev. Lett. **99**, 143903 (2007).
23. M. Xu, F. Yu, and J. Knight, "Mid-infrared 1W hollow-core fiber gas laser source," Opt. Lett. **42**, 4055-4058 (2017).